Growth Rate Dependence of Secondary Organic Aerosol on Seed Particle Size, Composition, and Phase

Devon N. Higgins, Michael S. Taylor, Jr., Justin M. Krasnomowitz, and Murray V. Johnston*

Department of Chemistry and Biochemistry, University of Delaware, Newark, Delaware, 19716, United States

KEYWORDS: Secondary Organic Aerosol (SOA), α-pinene, particle growth rate, particle-phase reactions, Aerosol Liquid Water (ALW), ultrafine particles, Aitken mode particles

ABSTRACT: The effects of composition, size, and phase state on ultrafine seed particle growth by α-pinene ozonolysis were determined from diameter growth measurements after a fixed reaction time in a flow tube reactor. Modeling time-dependent particle growth under a given set of conditions allowed the reaction growth factor (GF) to be determined, which is defined as the fraction of α-pinene molecules that react to give a product that grows the particles. Growth factors were compared for initial seed particle diameters of 40 nm, 60 nm, and 80 nm that were composed of freshly formed α-pinene SOA, effloresced ammonium sulfate, and deliquesced ammonium sulfate. Overall, SOA seed particles gave the lowest growth factors. Effloresced ammonium sulfate particles gave somewhat higher growth factors and showed a slight dependence on relative humidity. Deliquesced ammonium sulfate particles gave the highest growth factors. Seed particle size dependencies suggested that both surface- and volume- limited reactions may contribute to growth. Overall, the growth factors were found to vary by more than 4x across the reaction conditions studied. The results highlight the crucial role that seed particle characteristics play in determining particle growth rates in a size range relevant to formation of cloud condensation nuclei.

Introduction

Monoterpenes, a class of compounds such as α-pinene that are emitted by conifers and other vegetation, are important precursors for secondary organic aerosol (SOA) formation.[1] Monoterpenes are also key contributors to new particle formation and growth, especially in remote environments, because a significant portion of their oxidation products are non-volatile or semi-volatile.[2] Non-volatile products have low enough vapor pressures that they irreversibly condense onto preexisting particles or cluster with other molecular species to form new particles.[3] Semi-volatile products have higher vapor pressures, but still low enough that they partition into the condensed phase to contribute to particle growth.[4] It has been known for a long time that products of monoterpene oxidation can react in the condensed phase to form oligomers.[5] However, the ability of such reactions to contribute to particle growth is not fully understood and is likely to depend on the composition and phase state of the particles.[6]

Aerosol liquid water (ALW) can substantially alter the physicochemical properties of monoterpene SOA that affect the movement of molecules in and out of the particle phase. For example, Wilson et al.[7] measured changes in particle density using single particle mass spectrometry and found that ALW can act as a plasticizer in freshly generated α-pinene SOA, which helped reduce viscosity and enhance evaporation of semi-volatile material from the particle phase. The ability of ALW to decrease viscosity also has been shown by a decrease in particle bounce.[8] Since lowering the viscosity allows for faster molecular diffusion throughout the particle, ALW could enhance the absorption of semi-volatile molecules into the particle, allowing it to grow it faster than would otherwise be possible.[9,10] In addition, ALW can induce phase separation in particles, where a nonpolar organic layer forms on the outside of an aqueous inner layer, which may limit the fraction of the particle volume available to particle phase reactions or trap semi-volatile molecules inside the aqueous layer if the organic layer is extremely viscous and molecules cannot diffuse to the particle surface and escape.[11–13] Processes such as these can be inferred from evolution of the particle size distribution during a SOA formation experiment.[14]

ALW can provide a medium for aqueous phase reactions to occur. Li et al.[15] found that in the presence of ALW, the peroxide composition of α-pinene SOA was altered: they noticed an increase in H_2O_2 production while the total peroxide concentration remained unaffected. Wei et al.[16] found that peroxide functionalities in SOA from monoterpene ozonolysis can decompose in ALW to form OH and other species that, for example, may induce chemical aging of the aerosol. Aqueous phase reactions were reported by Zhao et al.[17] that increased the O/C ratio of α-pinene SOA, presumably as a result of hydrolysis reactions.[17]

The ability of ALW to alter aerosol growth was studied by Faust et al.[6] who reported a 13% enhancement in the amount of α-pinene SOA produced when the reaction is performed in the presence of deliquesced ammonium sulfate seed particles as opposed to effloresced seed particles. The study could not determine whether the enhancement was a result of increased partitioning of semi-volatile compounds into the aqueous volume, or the enabling of new chemical reactions within the aqueous volume. ALW can substantially enhance SOA formation from other precursors, most notably isoprene.[18] In addition to these laboratory studies, recent field measurements have linked ALW

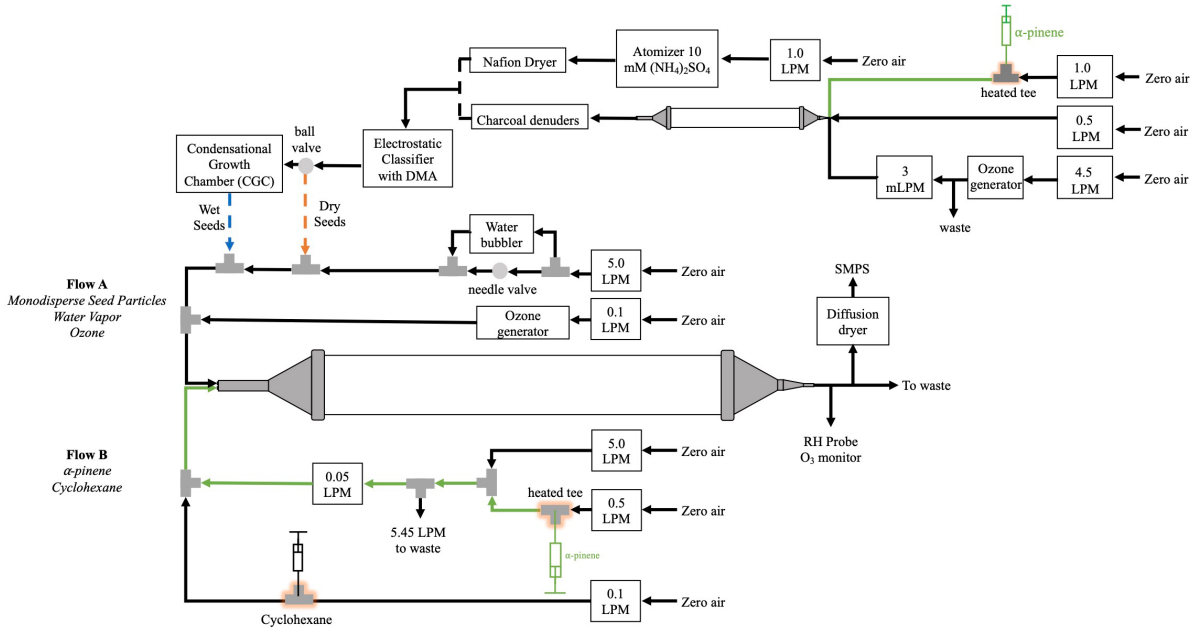

Figure 1. Schematic of the flow tube reactor and flow configurations used for this study. LPM = L/min; DMA = Differential Mobility Analyzer (TSI, Inc.); SMPS = Scanning Mobility Particle Sizer (TSI, Inc.)

with enhanced SOA formation on a regional scale.[19,20] The enhancement of SOA found in both laboratory and field investigations suggests that ALW may also impact the kinetics of particle growth. If so, ALW may increase the number of ultrafine particles that are able to grow into the CCN size range and thereby affect Earth's energy balance, though this possibility has not been systematically explored.

In the work presented here, the growth of α-pinene SOA is systematically studied as a function of seed particle size, composition, and phase, with a particular emphasis on ALW. Seed particles are generated, size-selected, and then mixed with α-pinene and ozone in a flow tube reactor.[21,22] The size range of interest, 40-100 nm dia., is within the Aitken mode size range of ambient aerosol where large numbers of particles exist and a small increase in particle size could have a large effect on CCN activity.[23] In the atmosphere, ALW mass typically exceeds that of dry aerosol mass by 2-3 times,[24] highlighting the need for a detailed understanding the effects of ALW on particle growth rate.

Experimental Methods

Flow Tube Reactor. The experimental setup for this study is illustrated in Figure 1. Seed particle growth by α-pinene ozonolysis was studied with a flow tube reactor described in detail by Krasnomowitz et al.[22] The reactor consists of a 20.0 cm diameter, 152 cm long quartz tube capped by two stainless steel funnels. Two separate flows were combined at the reactor inlet with a total flow rate through the reactor of 6.25 L/min. Flow A contained monodisperse seed particles, water vapor to control the RH, and ozone. Flow B contained α-pinene and cyclohexane, the latter added as an OH scavenger. The particle residence time in the flow tube was ~4 min. Aerosol exiting the reactor was continuously monitored with a Scanning Mobility Particle Sizer (SMPS; TSI, Inc.), an ozone monitor, (Model 49i, Thermo Fisher Scientific Inc.) and an RH probe (Traceable, Thermo Fisher Scientific Inc.).

Effloresced and Deliquesced Ammonium Sulfate Seed Particles. SOA growth on ammonium sulfate seed particles was studied under three different conditions: effloresced (dry) seed particles at 15% RH, effloresced (dry) seed particles at 60% RH, and deliquesced (wet) seed particles at 60% RH. The higher RH was maintained between the deliquescence and efflorescence relative humidity of ammonium sulfate, so that both dry and wet particles could be studied under otherwise identical conditions.

Initially, a polydisperse flow of seed particles was generated by atomizing (TOPAS ATM226, Dresden, Germany) a 10 mM solution of ammonium sulfate (99.9995%, Sigma-Aldrich Co., St. Louis, MO). The polydisperse flow passed through a Nafion dryer (MD-700, Perma Pure, Lakewood, NJ) to effloresce the particles, which were then size selected with a Model 3080 Classifier and Model 3085 Differential Mobility Analyzer (DMA) both from TSI Inc. (Shoreview, MN). When dry, effloresced particles at low RH were studied, this flow was mixed with ozone and sent into the flow tube reactor. For experiments with effloresced seed particles at high RH, this flow was mixed with humidified air to achieve 60% RH in the flow tube reactor. For experiments with deliquesced particles, the size selected dry seed particles were sent through a Condensational Growth Chamber (CGC, adapted from a customized device provided by Aerosol Dynamics Inc., Berkley, CA). The CGC exposed the particle flow to supersaturated water vapor, resulting in the condensation of liquid water onto the particles. These wet particles were then mixed with ozone and humidified air to achieve 60% RH in the reactor. For all experiments, the aerosol flow exiting the flow tube reactor was passed through a diffusion dryer to reduce the RH to ~15% and thereby remove ALW prior to

analysis with the SMPS. SMPS measurements were performed at low RH to ensure that the measured particle size is determined only by the non-volatile organic and inorganic matter in the particles as they exited the reactor, and not due to artifacts associated with changing amounts of ALW, since we found it difficult to keep the RH of the flow tube and SMPS identical. It is important to note that in similar experiments performed by Faust et al., water removal from the wet particles did not result in significant organic matter loss.[6]

Fresh α-Pinene SOA Seed Particles. Freshly generated seed particles composed of α-pinene secondary organic aerosol (SOA) were prepared using a small flow tube in line with the larger flow tube reactor described above. The small flow tube reactor is comprised of a 2.54 cm diameter, 130 cm long Teflon-lined stainless-steel tube.[25] Ozone (~15 ppmv) and α-pinene (1 ppmv) were mixed at the entrance of the flow tube, which had a residence time of ~30 s. SOA exiting the small flow tube was passed through charcoal denuders to remove ozone and excess gas-phase organics, then sent into a DMA for size selection. The monodisperse seed particles were sent directly into the large flow tube to be used in the growth experiments. Particle growth using these seeds was performed at both 15% and 60% RH.

Modelling Particle Growth. In the experiments described here, a monodisperse size-distribution of seed particles is grown by SOA formation, and the amount of growth is determined from the difference in median diameter of the *number* size distribution before and after SOA formation. Unfortunately, the diameter change for one type of experiment cannot be directly compared to that of another type because of the differences in particle size, number concentration, and therefore, condensation sink, for each experiment. For this reason, modeling must be performed to account for these effects. The approach adopted here is similar to that described in by Krasnomowitz et al.[22] which is itself based on a particle growth model described by Apsokardu and Johnston.[26] The model assumes that when α-pinene reacts with ozone, a significant fraction of these reaction events gives a product that is taken up by the particle, causing it to grow.

Here, we define condensed organic vapor (COV) collectively as the group of products that grew particles in a given experiment. In the context of partitioning theory, COV includes all non-volatile products that irreversibly condense onto the particle plus semi-volatile products that partition into the particle phase and stay there, at least for the duration of the experiment. It should be noted that COV is experiment dependent. For example, if growth of an unreactive seed particle is being studied, then initially only non-volatile products serve as COV. If growth of a reactive seed particle is being studied, then semi-volatile products may also contribute to COV if a significant fraction partitions into the particle and reacts to form non-volatile products. Differences in COV from one experiment to the next are summarized by the growth factor (GF), which is defined as the fraction of α-pinene ozonolysis events that gives a COV product. The goal of modelling is to determine GF for each individual experiment, since GF takes into account condensation sink and wall loss in the reactor.

First, the model iteratively calculates the time-dependent gas-phase COV concentration over the 4 min residence time of the flow tube (currently at 1 s time intervals). Then, the change in particle diameter at each time-point is calculated based on the collision-limited condensation of COV to the particle's surface, as shown by Equation 1:[26,27]

$$\frac{d(d_P)}{dt} = \frac{c}{2}\gamma[\mathrm{COV}]_t\beta_d V_{\mathrm{COV}} \quad (1)$$

where c is mean thermal velocity, γ is the uptake coefficient (assumed to be 1 in this work), $[COV]_t$ is the time-dependent gas-phase COV concentration, β_d is the correction factor for mass flux to a spherical particle with diameter d_P, and V_{COV} is the molecular COV volume. In these calculations, all COV molecules were assumed to have an average molecular weight of 200 g/mol and an average density of 1.2 g/cm^3. The processes which supply COV to and deplete COV from the system are accounted for when determining the COV concentration, as shown by Equation 2:

$$\frac{d[COV]_t}{dt} = (k_{II}[\alpha P]_g[O_3]_g)(GF) - k_{WL}[COV]_t - k_{CS}[COV]_t \quad (2)$$

COV is produced by the second order reaction between α-pinene and ozone with a molar yield given by the growth factor, GF (i.e. the molar yield of COV from the ozonolysis reaction is the same as GF defined in the previous paragraph) and k_{II} of 8.4 × 10^{-17} cm^3 molec^{-1} s^{-1}.[28] Two COV loss processes are also included in Equation 2. First, the rate of COV molecules lost to the flow tube walls is calculated as a diffusion limited process and follows Equation 3:[22]

$$k_{WL} = N_{\mathrm{Shw}}^{\mathrm{eff}}\frac{D}{r^2} \quad (3)$$

where k_{WL} is the wall loss constant, $N_{\mathrm{Shw}}^{\mathrm{eff}}$ is the effective Sherwood number, r is the radius of the flow tube, and D is the gas-phase diffusion coefficient, with the assumption that COV are non-volatile enough for the sticking probability to be 1. The average k_{WL} was determined by Krasnomowitz et al.[22] to be 2.0 × 10^{-3} s^{-1}. The second loss term is the rate of COV lost to the condensation sink according to Equation 4, which is adapted from the more familiar equation by Del Maso et al.[29] to reflect the monodisperse size distributions in these experiments:

$$k_{CS} = c\beta_d N_P(\pi/4)d_P^2 \quad (4)$$

where k_{CS} is the first-order rate of COV loss to the condensation sink, d_p is the median particle diameter, and N_p is the number concentration. As discussed by Krasnomowitz et al.[22] the condensation sink was calculated as a function of time in the flow tube as the aerosol grew from its initial to final diameter.

When deliquesced ammonium sulfate particles were modeled, the SMPS-measured dry median particle diameters were modified to include ALW. This was accomplished using E-AIM.[30–32] Initially, the number of moles of NH_4^+ and SO_4^{2-} present in the seed particle were calculated and from this, ALW was determined based on an RH of 60%. As the particles grew, the effect of SOA on ALW was estimated using glutaric acid as a proxy for the SOA. This calculation was repeated for each change in experimental conditions.

The only adjustable parameter in Equations 1-4 is GF, which was adjusted to fit the calculated increase in particle diameter to the measured median diameter increase of the size

distribution in each individual experiment. Because experiments were performed across a range of RH and seed particle size, composition and phase state, changes in the value of GF as a function of these parameters is able to give insight into processes associated with particle growth. Also, the modelling approach used in this study assumes GF to be constant over the entire time period of particle transit through the reactor.

An expanded discussion of the modeling approach is given in the Supporting Information including a derivation of Equation 1 and a validation test. This generic modeling approach is meant to determine how SOA growth depends on seed particle type without prior knowledge of the specific chemical mechanisms involved. It is not intended to be a detailed chemical model of SOA formation by α-pinene ozonolysis.

Safety Statement: Although no unexpected or unusually high safety hazards were encountered in this work, aerosols and ozone are inhalable hazards and care should be taken to ensure that flow lines and connectors are sealed and that the contents exiting the flow tube are properly filtered and exhausted.

Results and Discussion

The question this study seeks to answer is: How does particle growth in the Aitken mode size-range depend on seed particle size, composition, and/or phase state? The experimental approach is based on two key design elements. First, a monodisperse size-distribution of seed particles is grown. Second, growth is studied under conditions where the diameter increase of the particles is small. Studying growth of a monodisperse size-distribution provides the opportunity to use the generic growth model, described in the experimental section, which does not require prior knowledge of the specific chemical reactions occurring on the particle surface or inside the particle volume. Limiting the amount of growth is important because composition and phase may change as particles grow, meaning that the processes that control growth also may change substantially if too much growth occurs. These design elements are best achieved with a flow tube reactor, which allows a specific time-point in the reaction to be studied quantitatively. Additional discussion of the necessity for these design elements is given in Supporting Information.

Two types of experiments were performed. First are stepping experiments where the concentration of one reactant is systematically increased. These experiments provide the ability to effectively interrogate different time-points in the reaction since the reaction rate increases with increasing reactant concentration. Second are cycling experiments where the system is cycled back and forth between two specific reaction conditions, which provides the ability to quantitatively compare two reaction conditions at the same time-point. Results of both types of experiments are described below. The specific experiments performed are summarized in Tables S1 and S2.

Ozone Stepping Experiments. Ozone stepping experiments were conducted in a similar manner to those described in Krasnomowitz et al.[22] Initially, size-selected seed particles were mixed with the lowest ozone mixing ratio (~40 ppbv). After an equilibration period of approximately 1 hour, α-pinene (~11 ppbv) and cyclohexane (in excess; ~5.3 ppmv) were introduced into the flow tube reactor to initiate particle growth. After equilibration, the ozone mixing ratio was increased in five increments up to a maximum of ~200 ppbv. The experiment was performed for three size-selected particle diameters: 40, 60, and 80 nm. Table S1 summarizes the experiments and number of replicates that were performed. For experiments using deliquesced ammonium sulfate particles, the corresponding initial wet particle diameters (52, 78, and 104 nm) were reconstructed using E-AIM based on the dry seed particle diameters that were size-selected.[30–32]

Figure 2 shows representative data from an ozone stepping experiment using 40 nm effloresced ammonium sulfate seeds grown by α-pinene ozonolysis at 60% RH. The time course of the experiment is shown in Figure 2a. Ozone increments were performed at 1-hour intervals, which allowed the system to equilibrate (typically requires 30-45 min for our flow reactor) followed by a 15 min measurement interval over which the size distribution of aerosol exiting the reactor was averaged. The size distribution was characterized by median diameter, as this has been found to be a more precise measure of particle growth than, for example, particle volume concentration.[22] Precision is improved because median diameter does not depend on random fluctuations in number concentration. The measured size distribution shows no indication of particle nucleation as the ozone mixing ratio is incremented up. In Figure 2a, the lack of nucleation is indicated by an approximately constant number concentration throughout the experiment.

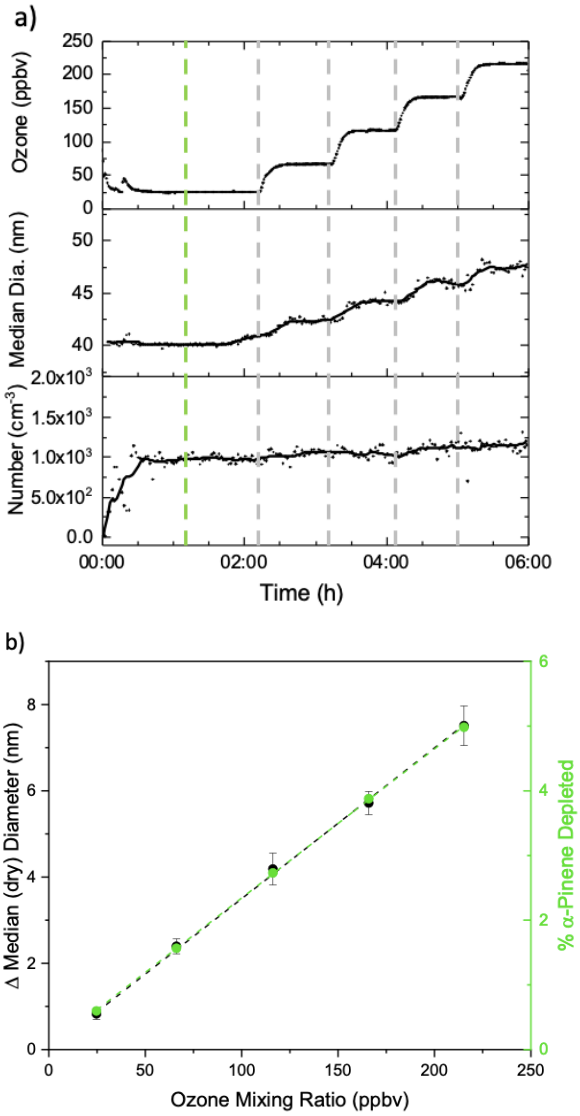

Figure 2. Representative data from an ozone stepping experiment using effloresced ammonium sulfate seed particles at 60% relative humidity. a) Ozone mixing ratio, median particle diameter, and number concentration vs. time. The green dashed line indicates the addition of α-pinene to the system, and each subsequent grey dashed line indicates an increase of ozone mixing ratio. b) Change in particle diameter (black) and percent of α-pinene that is depleted from the system (green) as a function of ozone mixing ratio for the same experiment; the dashed lines show linear regressions of the data.

Figure 2b shows plots of change in median particle diameter and % α-pinene depleted vs. ozone mixing ratio. Because the % α-pinene depleted is small, the plot is essentially linear with increasing ozone mixing ratio, meaning that the mixing ratio of oxidized products in the flow tube also increases linearly. The key features of the change in median diameter plot are its linearity and zero y-intercept. A linear relationship shows that particle growth is directly proportional to the amount of α-pinene precursor reacted, and it provides a level of confidence that a linear extrapolation back to lower, more atmospherically relevant conditions is possible. The lowest ozone mixing ratio give an average particle growth rate of ~15 nm/hr, whereas growth rates measured during new particle formation events are on the order of 1-10 nm/hr. Higher mixing ratios are generally preferred to use in flow tube experiments because reaction time is short, and the change in median diameter can be determined more precisely.

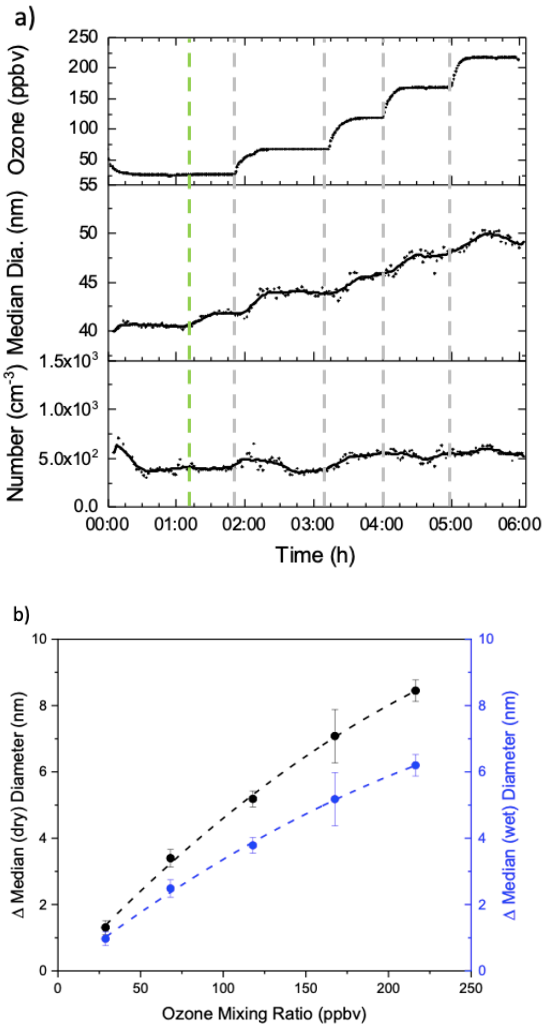

Figure 3. Representative data from an ozone stepping experiment using deliquesced ammonium sulfate seed particles at 60% relative humidity. a) Ozone mixing ratio, median dry particle diameter (measured by SMPS after the deliquesced particles were dried), and number concentration vs. time. Since the particles were deliquesced in this experiment, the actual median diameter of wet particles in the flow tube was greater than the measured dry diameter. The green dashed line indicates the addition of α-pinene to the system, and each subsequent grey dashed line indicates an increase of ozone mixing ratio. b) Change in dry particle diameter measured by SMPS (black) and the reconstructed change in wet particle diameter determined from E-AIM (blue) vs. ozone mixing ratio for the same experiment. Dashed curves are drawn as an aid to the eye.

Figure 3 shows a stepping experiment for growth of deliquesced ammonium sulfate seed particles at 60% RH. Recall that in this experiment, the SMPS measures dry particle diameter after water has been removed, whereas the deliquesced particles inside the flow tube are much larger. As with the effloresced particle experiment, increasing the ozone mixing ratio in the deliquesced particle experiment (Figure 3a) increases the median particle size, and no nucleation of new particles is observed. However, unlike the effloresced particle experiment, the plot of change in median dry diameter vs. ozone mixing ratio for the deliquesced particle experiment (Figure 3b) shows some curvature. This curvature is enhanced when E-AIM is used to reconstruct the change in median wet diameter that actually occurs inside the flow tube, also shown in Figure 3b. Figures 2b and 3b show that particle phase state can have a significant impact on growth by SOA from α-pinene ozonolysis. This dependence is discussed in greater detail in the following sections.

Cycling Experiments. The other type of experiment conducted in this study involved cycling between two seed particle conditions under otherwise identical growth conditions to quantitatively determine the impact of particle size, composition, and phase state on growth. Figure 4 shows the results of one such experiment where growth of deliquesced and effloresced AS particles were compared. In this experiment, 40 nm effloresced (dry) ammonium sulfate seed particles were size selected. Blue shaded regions in Figure 4 indicate time periods where the size selected particles were sent through the CGC to produce deliquesced particles (wet; blue dashed line of the experimental setup in Figure 1). Unshaded regions of the figure indicate time periods where effloresced particles were sent directly into the flow tube (red dashed line in Figure 1). The RH was maintained at 60% throughout this experiment. Initially, dry particles were sent through the flow tube, and then wet particles without any SOA formation. Although both types of particles exiting the flow reactor were sent through a diffusion drier to remove any ALW before SMPS analysis (RH <15%), the deliquesced particles showed a slightly larger (dry) particle diameter than the effloresced particles – a phenomenon that was observed in all of our experiments using deliquesced seeds. This effect has been observed before and has been attributed to particle restructuring upon drying.[33] The vertical green dashed line in Figure 4 shows the time-point at which α-pinene was sent into the flow tube to produce SOA. The particle size increased, and after an equilibration period of approximately one hour, the seed particle flow was switched to effloresced particles. After another equilibration period, the process was repeated. Median (dry) diameters for each equilibration period were averaged over the final 15 min of the period prior to switching to the new period. The average median diameters are shown in the top plot

of Figure 4 as solid horizontal lines, illustrating the consistency of diameter measurement from one "identical" period to the next.

Cycling the seed particles in this manner assured that both types of particles (effloresced and deliquesced for Figure 4) were exposed to precisely same conditions: 60% RH, ozone mixing ratio 200 ppbv, α-pinene mixing ratio ~11 ppbv, and cyclohexane mixing ratio ~5.3 ppmv (in excess in the experiment). Most of the key reaction conditions were measured directly, with the notable exception of α-pinene mixing ratio. The α-pinene mixing ratio was calculated from the liquid injection rate of α-pinene and subsequent dilution of the vapor (Figure 1), and in principle can vary slightly from experiment to experiment if the liquid feed rate fluctuates due to residue buildup in the injection apparatus. For this reason, cycling experiments were performed for quantitative comparisons.

The diameter changes obtained from this experiment cannot be directly compared for effloresced and deliquesced seed particles because the condensation sink is very different for the two. As shown in the middle plot of Figure 4, sending the aerosol flow through the CGC resulted in a significant loss of particles, which affected the CS (bottom plot of Figure 4, calculated from the size distribution in the final 15 min of each equilibration period) and hence the magnitude of the diameter growth. The difference in condensation sink is taken into account by the modelling procedure to determine GF. Experiments similar to that in Figure 4 were performed to compare growth for various combinations of seed particle composition, size, and phase state. Table S2 lists the experiments performed, the number of cycles and replicates for each, and the relative growth factors determined from modeling the amount of growth observed.

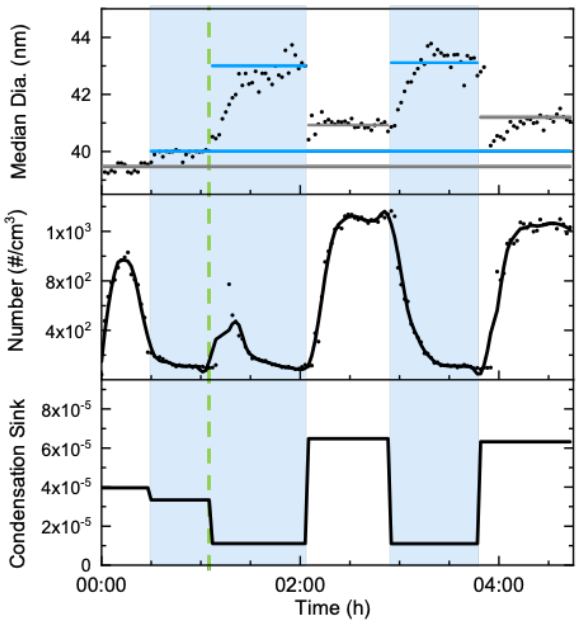

Figure 4. Representative data from a cycling experiment performed at 60% RH where nominally 40 nm dry ammonium sulfate particles were size selected and SOA growth was compared for deliquesced vs. effloresced seed particles. Blue shaded regions indicate time periods where deliquesced particles were sent through the flow tube, while unshaded regions indicate time periods where effloresced particles were sent through the flow tube. The green dashed line indicates the time at which α-pinene began to flow through the system to produce SOA. The top plot shows the *dry* median diameter of aerosol measured by SMPS; horizontal lines show the average of the final 15 min of each period. The middle plot shows the number concentration. The bottom plot shows the condensation sink (CS) determined from the SMPS size distribution averaged over the final 15 min of each equilibration period, and for deliquesced particles using E-AIM to account for ALW.

Relative Growth Factors. Growth Factor (GF) is the fraction of α-pinene ozonolysis products able to grow a particle in a given experiment. As described in the experimental section, this includes all non-volatile ozonolysis products plus the portion of semi-volatile products able to react on the particle surface or in the particle volume to form a non-volatile product. GF is calculated from the measured diameter change, but is relatively unaffected by wall loss and magnitude of the condensation sink. Each cycling experiment provides a measure of two GF values, for example effloresced vs. deliquesced particles in Figure 4, and from these, the ratio of the two GF values is determined. When the results of many cycling experiments are combined (see Table S2), GF can be quantitatively compared over a wide range of particle growth conditions.

Figure 5 plots Relative Growth Factor, calculated with respect to 40 nm α-pinene ozonolysis SOA particles grown at low RH, vs. initial dry seed particle diameter. In general, GF is smallest for SOA seed particles, somewhat higher for effloresced ammonium sulfate particles, and greatest for deliquesced ammonium sulfate particles. GF is generally the same for 40 nm vs. 60 nm dia, seed particles of a given composition and phase. GF increases for 80 nm liquid-like particles (SOA and deliquesced ammonium sulfate), while GF for effloresced ammonium sulfate particles at low and high RH remain flat. The results show that SOA growth strongly depends on seed particle size, composition, and phase state.

SOA seed particle growth in this study is similar to previously reported chamber experiments where α-pinene ozonolysis caused both nucleation and subsequent growth of SOA particles.[3,34] The chamber experiments showed that growth in the low nm size range occurred mainly by condensation of extremely low volatility, highly oxidized organic compounds (HOMs), which were formed by gas-phase autooxidation of peroxy radicals produced by α-pinene ozonolysis. The HOM yield in those experiments was reported to be on the order of 6-8%.[3,34] We suggest that the absolute GF for 40 and 60 nm SOA particles in Figure 5 is in fact the HOM yield. The increase in GF for 80 nm particles indicates that semi-volatile compounds are able to react within the particle phase to form low volatility products and thereby remain in the particle phase rather than partitioning back to the gas phase. Previous modelling by our group shows that particle growth due to oligomerization can increase with increasing particle size if oligomer formation is a volume-limited process.[26] Experimental measurements of size-selected SOA particles produced by α-pinene[35] and β-pinene[36] ozonolysis confirm that oligomerization does indeed increase with increasing particle size. Based on these studies, the increase of GF for 80 nm SOA seed particles is likely a consequence of semi-volatile compound oligomerization in the particle phase. Also shown in Figure 5 is that GFs for SOA seed particles are the same for 15% and 60% RH. The lack of an RH dependence for growth indicates that under the conditions of

our experiments, both HOM formation and wall effects are independent of RH.[37]

Effloresced ammonium sulfate particle growth at low RH in this study is similar to our previous work, where modelling of ozone stepping experiments gave an absolute GF of 13%[22]. A GF of this magnitude is consistent with Figure 5, where the relative growth factor of effloresced ammonium sulfate particles is about 1.5 to 2 times larger than that of SOA particles. The higher GF relative to SOA particles is likely due to chemical processes on the ammonium sulfate surface that allow semi-volatile ozonolysis products to be transformed into non-volatile secondary products. Likely possibilities include oligomerization and organosulfate formation. It should be noted that surface water exists on a "dry" ammonium sulfate substrate, ranging from <1 monolayer at 10% RH to 3-5 monolayers at 60% RH.[38,39] This aqueous film may provide a medium for interfacial chemistry to occur,[40] which is consistent with the slightly higher GF at 60% RH than 15% RH as well as the higher GF than SOA seed particles. This film is also likely to be acidic,[41,42] a property which is known catalyze relevant particle phase reactions.[5,43,44]

Figure 5 also shows that deliquesced ammonium sulfate particle growth is substantially greater than that of either SOA or effloresced ammonium sulfate particles. Deliquesced particles provide the opportunity for aqueous phase chemistry in the particle volume as well as chemistry at the interface. In addition to oligomerization and organosulfate formation, hydroperoxide products of α-pinene ozonolysis could decompose in the aqueous phase to produce hydroxyl radicals that oxidize semi-volatile products that have partitioned. Enhanced formation of α-pinene SOA on deliquesced ammonium sulfate seed particles has also been reported by Faust et al.,[6] who found a 13% enhancement relative to effloresced seeds as determined by ToF-AMS measurements. The magnitude of their increase is not directly comparable to ours because of different reaction conditions for the two experiments.

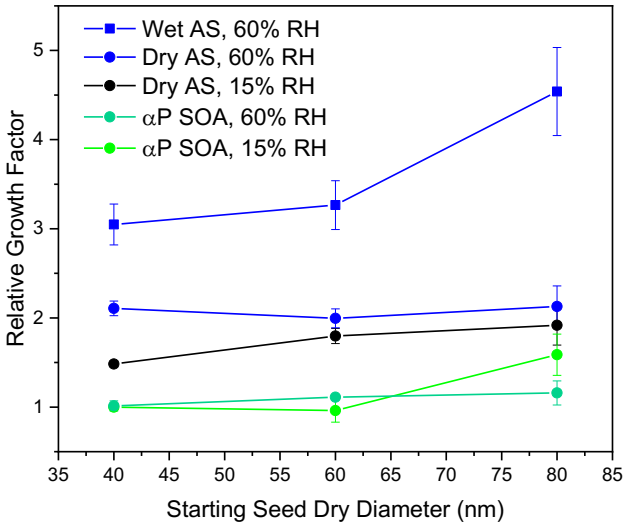

Figure 5. Relative Growth Factor (referenced to 40 nm dia. α-pinene ozonolysis SOA seed particles) vs. starting seed particle size for five reaction conditions: SOA at 15% RH, SOA at 60% RH, effloresced ammonium sulfate at 15% RH, effloresced ammonium sulfate at 60% RH, and deliquesced ammonium sulfate at 60% RH.

Deliquesced ammonium sulfate particles are different from SOA and effloresced ammonium sulfate particles in that the diameter change during growth is not linearly related to the ozone mixing ratio (Figure 3b). Since the results in Figure 5 were obtained for a high ozone mixing ratio, the vertical location of deliquesced ammonium sulfate particles on this plot will likely increase with decreasing ozone mixing ratio. This point is explored further in Figure 6, where the data in Figures 2b and 3b are used to construct plots of GF vs. ozone mixing ratio. In this figure, the GF values are referenced to the low-end ozone mixing ratio. For effloresced seed particles, the diameter change plot in Figure 2b suggests that the GF is independent of ozone mixing ratio, which is shown to the be case in Figure 6. The slight fluctuation of effloresced seed particle GF in Figure 6 is caused by uncertainty in the SMPS median diameter measurements. For deliquesced seed particles, the diameter change plot in Figure 3b suggests that GF decreases with increasing ozone mixing ratio, which is evident in Figure 6, where the 20% decrease of GF over the range of ozone mixing ratios plotted is significantly outside the measurement uncertainty of SMPS. We suggest two possibilities for this decrease. First, an organic film may grow on the particle surface, which blocks any contribution to particle growth from surface chemistry but still allows chemistry within the particle volume to occur. Second, chemical processes within the particle volume may be impeded by the increasing organic content of the aqueous phase as the ozone mixing ratio increases and more SOA is produced. The GF decrease for deliquesced particles is not an artifact of water evaporation from the particle as SOA is formed. E-AIM modeling (Figure S3) shows that while the percentage of ALW by volume decreases as the SOA content increases, the absolute amount of water in the particle increases slightly, as expected.

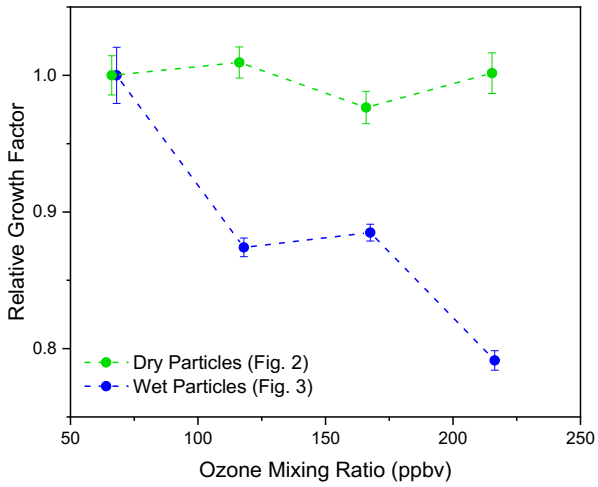

Figure 6. Relative Growth Factor vs. ozone mixing ratio for the effloresced ammonium sulfate particles in Figure 2 (green) and the deliquesced ammonium sulfate particles in Figure 3 (blue), both referenced to the GF for the lowest ozone mixing ratio plotted.

In conclusion, the work presented here shows that ultrafine particle growth by α-pinene SOA formation is strongly dependent upon seed particle size, composition, and phase state. Future work should focus on elucidating the specific chemical processes contributing to these dependencies, as well as to characterize the seed particle dependence of SOA formation from other precursors. Finally, we note that ammonium sulfate particles generated with an atomizer may contain unknown organic impurities,[45] and indeed a trace carbon contamination is observed with our nano aerosol mass spectrometer.[46] The ability

of such contamination to influence particle growth should be investigated.

ASSOCIATED CONTENT

Supporting Information

The Supporting Information is available free of charge on the ACS Publications website.

This information includes an extended description of the modeling approach. Three figures are provided: illustration of the modeling approach (Figure S1), a test of the approach using GFs obtained from modeling diameter changes from *volume* size-distributions (Figure S2), and E-AIM modeling of the water content of deliquesced ammonium sulfate particles as they grow by SOA formation (Figure S3). Tabulated lists are provided for the Ozone Stepping Experiments (Table S1) and Cycling Experiments (Table S2) performed in this work.

AUTHOR INFORMATION

Corresponding Author

*Murray V. Johnston – Department of Chemistry and Biochemistry, University of Delaware, Newark, Delaware, 19716, United States; Email: mvj@udel.edu

ORCID

Devon N. Higgins: 0000-0003-1147-1724

Michael S. Taylor, Jr.: 0000-0003-0913-7284

Justin M. Krasnomowitz: 0000-0002-3929-6879

Murray V. Johnston: 0000-0001-9529-8660

Author Contributions

All authors have given approval to the final version of the manuscript.

Notes

The authors declare no competing financial interests.

ACKNOWLEDGMENT

This research was supported by two grants from the U.S. National Science Foundation, CHE-1904765 and AGS-1916819.

ABBREVIATIONS

COV, condensed organic vapor; GF, growth factor.

REFERENCES

(1) Sindelarova, K.; Granier, C.; Bouarar, I.; Guenther, A.; Tilmes, S.; Stavrakou, T.; Müller, J. F.; Kuhn, U.; Stefani, P.; Knorr, W. Global Data Set of Biogenic VOC Emissions Calculated by the MEGAN Model over the Last 30 Years. *Atmos. Chem. Phys.* **2014**, *14* (17), 9317–9341.

(2) Trump, E. R.; Donahue, N. M. Oligomer Formation within Secondary Organic Aerosols: Equilibrium and Dynamic Considerations. *Atmos. Chem. Phys.* **2014**, *14* (7), 3691–3701.

(3) Ehn, M.; Thornton, J. A.; Kleist, E.; Sipilä, M.; Junninen, H.; Pullinen, I.; Springer, M.; Rubach, F.; Tillmann, R.; Lee, B.; et al. A Large Source of Low-Volatility Secondary Organic Aerosol. *Nature* **2014**, *506* (7489), 476–479.

(4) Donahue, N. M.; Kroll, J. H.; Pandis, S. N.; Robinson, A. L. A Two-Dimensional Volatility Basis Set-Part 2: Diagnostics of Organic-Aerosol Evolution. *Atmos. Chem. Phys.* **2012**, *12* (2), 615–634.

(5) Tolocka, M. P.; Jang, M.; Ginter, J. M.; Cox, F. J.; Kamens, R. M.; Johnston, M. V. Formation of Oligomers in Secondary Organic Aerosol. *Environ. Sci. Technol.* **2004**, *38* (5), 1428–1434.

(6) Faust, J. A.; Wong, J. P. S.; Lee, A. K. Y.; Abbatt, J. P. D. Role of Aerosol Liquid Water in Secondary Organic Aerosol Formation from Volatile Organic Compounds. *Environ. Sci. Technol.* **2017**, *51* (3), 1405–1413.

(7) Wilson, J.; Imre, D.; Beránek, J.; Shrivastava, M.; Zelenyuk, A. Evaporation Kinetics of Laboratory-Generated Secondary Organic Aerosols at Elevated Relative Humidity. *Environ. Sci. Technol.* **2015**, *49* (1), 243–249.

(8) Slade, J. H.; Ault, A. P.; Bui, A. T.; Ditto, J. C.; Lei, Z.; Bondy, A. L.; Olson, N. E.; Cook, R. D.; Desrochers, S. J.; Harvey, R. M.; et al. Bouncier Particles at Night: Biogenic Secondary Organic Aerosol Chemistry and Sulfate Drive Diel Variations in the Aerosol Phase in a Mixed Forest. *Environ. Sci. Technol.* **2019**, *53* (9), 4977–4987.

(9) Zaveri, R. A.; Shilling, J. E.; Zelenyuk, A.; Zawadowicz, M. A.; Suski, K.; China, S.; Bell, D. M.; Veghte, D.; Laskin, A. Particle-Phase Diffusion Modulates Partitioning of Semivolatile Organic Compounds to Aged Secondary Organic Aerosol. *Environ. Sci. Technol.* **2020**, *54* (5), 2595–2605.

(10) Hosny, N. A.; Fitzgerald, C.; Vyšniauskas, A.; Athanasiadis, A.; Berkemeier, T.; Uygur, N.; Pöschl, U.; Shiraiwa, M.; Kalberer, M.; Pope, F. D.; et al. Direct Imaging of Changes in Aerosol Particle Viscosity upon Hydration and Chemical Aging. *Chem. Sci.* **2016**, *7* (2), 1357–1367.

(11) Freedman, M. A. Phase Separation in Organic Aerosol. *Chem. Soc. Rev.* **2017**, *46* (24), 7694–7705.

(12) Vander Wall, A. C.; Perraud, V.; Wingen, L. M.; Finlayson-Pitts, B. J. Evidence for a Kinetically Controlled Burying Mechanism for Growth of High Viscosity Secondary Organic Aerosol. *Environ. Sci. Process. Impacts* **2020**, *22* (1), 66–83.

(13) Vander Wall, A. C.; Wingen, L. M.; Perraud, V.; Zhao, Y.; Finlayson-Pitts, B. J. Enhanced Gas Uptake during α-Pinene Ozonolysis Points to a Burying Mechanism. *ACS Earth Sp. Chem.* **2020**, *4* (8), 1435–1447.

(14) He, Y.; Akherati, A.; Nah, T.; Ng, N. L.; Garofalo, L. A.; Farmer, D. K.; Shiraiwa, M.; Zaveri, R. A.; Cappa, C. D.; Pierce, J. R.; et al. Particle Size Distribution Dynamics Can Help Constrain the Phase State of Secondary Organic Aerosol. *Environ. Sci. Technol.* **2021**.

(15) Li, H.; Chen, Z.; Huang, L.; Huang, D. Organic Peroxides' Gas-Particle Partitioning and Rapid Heterogeneous Decomposition on Secondary Organic Aerosol. *Atmos. Chem. Phys.* **2016**, *16* (3), 1837–1848.

(16) Wei, J.; Fang, T.; Wong, C.; Lakey, P. S. J.; Nizkorodov, S. A.; Shiraiwa, M. Superoxide Formation from Aqueous Reactions of Biogenic Secondary Organic Aerosols. *Environ. Sci. Technol.* **2021**, *55* (1), 260–270.

(17) Zhao, Z.; Le, C.; Xu, Q.; Peng, W.; Jiang, H.; Lin, Y. H.; Cocker, D. R.; Zhang, H. Compositional Evolution of Secondary Organic Aerosol as Temperature and Relative Humidity Cycle in Atmospherically Relevant Ranges. *ACS Earth Sp. Chem.* **2019**, *3* (11), 2549–2558.

(18) Wong, J. P. S.; Lee, A. K. Y.; Abbatt, J. P. D. Impacts of Sulfate Seed Acidity and Water Content on Isoprene Secondary Organic Aerosol Formation. *Environ. Sci. Technol.* **2015**, *49* (22), 13215–13221.

(19) Carlton, A. G.; Christiansen, A. E.; Flesch, M. M.; Hennigan, C. J.; Sareen, N. Mulitphase Atmospheric Chemistry in Liquid Water: Impacts and Controllability of Organic Aerosol. *Acc. Chem. Res.* **2020**, *53* (9), 1715–1723.

(20) Zhang, J.; Lance, S.; Marto, J.; Sun, Y.; Ninneman, M.; Crandall, B. A.; Wang, J.; Zhang, Q.; Schwab, J. J. Evolution of Aerosol Under Moist and Fog Conditions in a Rural Forest Environment: Insights From High-Resolution Aerosol Mass Spectrometry. *Geophys. Res. Lett.* **2020**, *47* (19).

(21) Stangl, C. M.; Krasnomowitz, J. M.; Apsokardu, M. J.; Tiszenkel, L.; Ouyang, Q.; Lee, S.; Johnston, M. V. Sulfur Dioxide Modifies Aerosol Particle Formation and Growth by Ozonolysis of Monoterpenes and Isoprene. *J. Geophys. Res. Atmos.* **2019**, *124* (8), 4800–4811.

(22) Krasnomowitz, J. M.; Apsokardu, M. J.; Stangl, C. M.; Ouyang, Q.; Lee, S.; Johnston, M. V; Krasnomowitz, J. M.; Apsokardu, M. J.; Stangl, C. M.; Tiszenkel, L.; et al. Growth of Aitken Mode Ammonium Sulfate Particles by α -Pinene Ozonolysis. *Aerosol Sci. Technol.* **2019**, *53* (4), 406–419.
(23) Dusek, U.; Frank, G. P.; Hildebrandt, L.; Curtius, J.; Schneider, J.; Walter, S.; Chand, D.; Drewnick, F.; Hings, S.; Jung, D.; et al. Size Matters More Than Chemistry Aerosol Particles. *Science (80-.).* **2006**, *312* (5778), 1375–1378.
(24) Ervens, B.; Turpin, B. J.; Weber, R. J. Secondary Organic Aerosol Formation in Cloud Droplets and Aqueous Particles (AqSOA): A Review of Laboratory, Field and Model Studies. *Atmos. Chem. Phys.* **2011**, *11* (21), 11069–11102.
(25) Heaton, K. J.; Dreyfus, M. A.; Wang, S.; Johnston, M. V. Oligomers in the Early Stage of Biogenic Secondary Organic Aerosol Formation and Growth. *Environ. Sci. Technol.* **2007**, *41* (17), 6129–6136.
(26) Apsokardu, M. J.; Johnston, M. V. Nanoparticle Growth by Particle-Phase Chemistry. *Atmos. Chem. Phys.* **2018**, *18* (3), 1895–1907.
(27) Weber, R. J.; Marti, J. J.; McMurry, P. H.; Eisele, F. L.; Tanner, D. J.; Jefferson, A. Measured Atmospheric New Particle Formation Rates: Implications for Nucleation Mechanisms. *Chem. Eng. Commun.* **1996**, *151* (January 2015), 53–64.
(28) Khamaganov, V. G.; Hites, R. A. Rate Constants for the Gas-Phase Reactions of Ozone with Isoprene, α- and β-Pinene, and Limonene as a Function of Temperature. *J. Phys. Chem. A* **2001**, *105* (5), 815–822.
(29) Dal Maso, M.; Kulmala, M.; Lehtinen, K. E. J.; M̈kelä, J. M.; Aalto, P.; O'Dowd, C. D. Condensation and Coagulation Sinks and Formation of Nucleation Mode Particles in Coastal and Boreal Forest Boundary Layers. *J. Geophys. Res. Atmos.* **2002**, *107* (19).
(30) Clegg, S. L.; Brimblecombe, P.; Wexler, A. S. Thermodynamic Model of the System H+-NH4+-SO42-NO 3--H2O at Tropospheric Temperatures. *J. Phys. Chem. A* **1998**, *102* (12), 2137–2154.
(31) Wexler, A. S.; Clegg, S. L. Atmospheric Aerosol Models for Systems Including the Ions H+, NH4+, Na+, So42-, NO 3-, Cl-, Br-, and H2O. *J. Geophys. Res. Atmos.* **2002**, *107* (14).
(32) Clegg, S. L.; Seinfeld, J. H.; Edney, E. O. Thermodynamic Modelling of Aqueous Aerosols Containing Electrolytes and Dissolved Organic Compounds. II. An Extended Zdanovskii-Stokes-Robinson Approach. *J. Aerosol Sci.* **2003**, *34* (6), 667–690.
(33) Mikhailov, E.; Vlasenko, S.; Martin, S. T.; Koop, T.; Pöschl, U. Amorphous and Crystalline Aerosol Particles Interacting with Water Vapor: Conceptual Framework and Experimental Evidence for Restructuring, Phase Transitions and Kinetic Limitations. *Atmos. Chem. Phys.* **2009**, *9* (24), 9491–9522.
(34) Bianchi, F.; Kurtén, T.; Riva, M.; Mohr, C.; Rissanen, M. P.; Roldin, P.; Berndt, T.; Crounse, J. D.; Wennberg, P. O.; Mentel, T. F.; et al. Highly Oxygenated Organic Molecules (HOM) from Gas-Phase Autoxidation Involving Peroxy Radicals: A Key Contributor to Atmospheric Aerosol. *Chem. Rev.* **2019**, *119* (6), 3472–3509.
(35) Kerecman, D. E.; Apsokardu, M. J.; Talledo, S. L.; Taylor, M. S.; Haugh, D. N.; Zhang, Y.; Johnston, M. V. Online Characterization of Organic Aerosol by Condensational Growth into Aqueous Droplets Coupled with Droplet-Assisted Ionization. *Anal. Chem.* **2021**, *93* (5), 2793–2801.
(36) Tu, P.; Johnston, M. V. Particle Size Dependence of Biogenic Secondary Organic Aerosol Molecular Composition. *Atmos. Chem. Phys.* **2017**, *17* (12), 7593–7603.
(37) Li, X.; Chee, S.; Hao, J.; Abbatt, J. P. D.; Jiang, J.; Smith, J. N. Relative Humidity Effect on the Formation of Highly Oxidized Molecules and New Particles during Monoterpene Oxidation. **2019**, 1555–1570.
(38) Hsiao, T. C.; Young, L. H.; Tai, Y. C.; Chen, K. C. Aqueous Film Formation on Irregularly Shaped Inorganic Nanoparticles before Deliquescence, as Revealed by a Hygroscopic Differential Mobility Analyzer–Aerosol Particle Mass System. *Aerosol Sci. Technol.* **2016**, *50* (6), 568–577.
(39) Xu, J.; Imre, D.; McGraw, R.; Tang, I. Ammonium Sulfate: Equilibrium and Metastability Phase Diagrams from 40 to -50°C. *J. Phys. Chem. B* **1998**, *102* (38), 7462–7469.
(40) Kong, X.; Castarède, D.; Thomson, E. S.; Boucly, A.; Artiglia, L.; Ammann, M.; Gladich, I.; Pettersson, J. B. C. *Science*. **2021**, *752* (November), 747–752.
(41) Huang, Q.; Wei, H.; Marr, L. C.; Vikesland, P. J. Direct Quantification of the Effect of Ammonium on Aerosol Droplet PH. *Environ. Sci. Technol.* **2021**, *55* (1), 778–787.
(42) Hua, W.; Verreault, D.; Allen, H. C. Relative Order of Sulfuric Acid, Bisulfate, Hydronium, and Cations at the Air-Water Interface. *J. Am. Chem. Soc.* **2015**, *137* (43), 13920–13926.
(43) Surratt, J. D.; Lewandowski, M.; Offenberg, J. H.; Jaoui, M.; Kleindienst, T. E.; Edney, E. O.; Seinfeld, J. H. Effect of Acidity on Secondary Organic Aerosol Formation from Isoprene. *Environ. Sci. Technol.* **2007**, *41* (15), 5363–5369.
(44) Surratt, J. D.; Kroll, J. H.; Kleindienst, T. E.; Edney, E. O.; Claeys, M.; Sorooshian, A.; Ng, N. L.; Offenberg, J. H.; Lewandowski, M.; Jaoui, M.; et al. Evidence for Organosulfates in Secondary Organic Aerosol. *Environ. Sci. Technol.* **2007**, *41* (2), 517–527.
(45) Wu, J.; Brun, N.; Gonzá, J. M.; Mili, B. R.; Roussel, B. T.; Ravier, S.; Clé, J.; Monod, A. Substantial Organic Impurities at the Surface of Synthetic Ammonium Sulfate Particles. **2022**, No. 15, 3859–3874.
(46) Horan, A. J.; Krasnomowitz, J. M.; Johnston, M. V. Particle Size and Chemical Composition Effects on Elemental Analysis with the Nano Aerosol Mass Spectrometer. *Aerosol Sci. Technol.* **2017**, *51* (10), 1135–1143.

Insert Table of Contents artwork here